Influence of annealing on the properties of chemically prepared SnS thin films

S. John[a,b,*], M. Francis[b], A. P. Reena Mary[a], V. Geetha[a]
*[a]Department of Physics, Govt.Victoria College (affiliated to University of Calicut)
Palakkad Kerala 678001, India*
*[b]Department of Physics, Mercy College (affiliated to University of Calicut)
Palakkad Kerala 678006, India*

Thin films of SnS were deposited chemically, and they are annealed at four different temperatures: 100 °C, 150 °C, 200 °C, and 250 °C. X-ray diffraction, Raman analysis, UV-visible spectroscopy, field emission scanning electron microscopy, and energy dispersive spectroscopy were used to investigate the impact of annealing temperature on the structural, optical, morphological, and chemical properties of thin films. As the annealing temperature rose, it was seen from the XRD patterns that the crystallinity of SnS films improved. At 250 °C, the film was almost evaporated, and the XRD pattern showed no peaks at all. The lattice strain and crystallite size were computed from the Williamson-Hall plots. The crystallite size increased and the lattice strain decreased with the increase in the annealing temperature. According to optical investigations, the samples' optical bandgap shrank as the annealing temperature rose. Morphological studies showed the formation of well-adhered films, and as the annealing temperature increased, the film became denser and more continuous with larger grains. The atomic weight percentage of sulphur decreased as the annealing temperature increased, according to the EDS analysis. Photovoltaic structures with the configuration ITO/SnS/CdS/Ag were fabricated. From the I-V characteristics, it was observed that the cell structure formed with SnS annealed at 200 °C showed better cell performance.

1. Introduction

Thin-film solar cells (TFSCs) are becoming more popular due to their flexibility, low cost, and ease of production. But compared to its crystalline counterparts, its efficiency has remained lower. As they are the least expensive choice, numerous research projects are carried out to increase the thin film solar cells' efficiency. SnS, a semiconductor from the IV-VI group, is a promising absorber layer for solar cells. It is an easy-to-use, non-toxic substance that is common on Earth. It also has a high absorption coefficient ($\sim 10^5$ cm^{-1}) and p type conductivity. For orthorhombic SnS, the direct and indirect band gaps are, respectively, 1.3-1.5 eV and 1.0-1.1 eV. Theoretical research by Loferski [6] and Abdul Kuddus et al. [7] has demonstrated that solar cells based on SnS have a maximum conversion efficiency of above 20%. All of these factors imply that SnS may be used as an absorber layer in thin-film solar cells. But the maximum reported efficiency for SnS-based solar cells is 4.6% [1]. There are many challenges on the way to improving conversion efficiency, like choosing the proper window layer, making good quality SnS layers, improving the output circuit voltage of the cell, and enhancing the light trapping within the cell [2]. The challenge of creating high-quality SnS must be resolved in order to create high-efficiency SnS-based solar cells.

SnS thin films have been deposited using a variety of techniques, such as vacuum evaporation. [3], [4], sputtering [5], [6], CVD [7], [8], electrodeposition [9], [10], pulsed-laser deposition [11], [12], spray pyrolysis [13], [14], SILAR [15], [16], and chemical bath deposition (CBD) [17], [18]. CBD is one of the most widely used synthesis routes for the creation of

inorganic metal chalcogenide and oxide semiconductor thin films due to its many advantages, including large area deposition, comparatively low-temperature processes, a lack of substrate use constraints, reproducibility, and most especially, low equipment cost [19].

Various scholars have claimed that the structural, optical, morphological, and chemical characteristics of the various constituent layers have an impact on the efficiency of thin film solar cells, especially the absorber layer [20]. T. Ben. Nasr et al. [21] suggested that the physical properties of the ZnS thin film can be modulated, and Melda Francis et al. [22] studied the effect of annealing on the structural and optical properties of the chemically prepared Cu_2Se thin films. In this work, SnS thin films were prepared chemically and annealed at four different temperatures. The effect of annealing temperature on the properties of SnS thin film was investigated. SnS/CdS heterojunctions were fabricated, and the performance of the cells was also evaluated.

2. Experimental methods

2.1. Preparation of SnS thin films

Stannous chloride ($SnCl_2.2H_2O$) and thioacetamide (CH_3CSNH_2) were utilised in this study as precursors for tin and sulphur, respectively. Triethanolamine $N(CH_2CH_2OH)_3$ (TEA) and trisodium citrate $Na_3C_6H_5O_7.2H_2O$ (TSC) were used as complexing agents to slow down the reaction rate and prevent abrupt precipitation. The analytical grade compounds used in this investigation were all bought from Merck. First, 5 ml of 0.6 M trisodium citrate was mixed with 0.3 M $SnCl_2.2H_2O$ dissolved in glacial acetic acid. Next, 5 ml of TEA and 5 ml of 0.1 M thioacetamide were added. The pH of the bath solution was determined to be 10 after 4 ml of a 0.91 Sp. Gr ammonia solution was added. Glass substrates that had been completely cleaned were submerged in the final solution after the requisite amount of ammonia had been added. The final solution had been brought to 100 ml by the addition of deionized water. The initially clear solution darkened gradually to yellow, then to chocolate brown. After six hours at room temperature, the SnS thin film with a dark brown colour was produced. The films were characterized after a half hour of annealing at 100 °C, 150 °C, 200 °C, and 250 °C

2.2. Fabrication of SnS/CdS photovoltaic cell

CdS thin films were prepared from a chemical bath containing 0.1 M cadmium acetate (($CH_3COO)_2Cd.2H_2O$) as a cationic precursor, 0.3 M thiourea as an anionic precursor, triethanolamine (TEA) as a complexing agent, and ammonium hydroxide (NH_4OH) as a buffer solution [23] . The prepared CdS thin films were yellow in colour and were homogeneous, smooth, and adherent to the substrate. The heterojunction was formed on a thoroughly cleaned ITO substrate. Firstly, the SnS thin film was coated and annealed as mentioned before, followed by the deposition of CdS. A thin silver contact was drawn above the heterojunction using silver paste. The I-V characteristics were studied using a Keithley source meter.

3. Results and discussion

Utilizing a Cu Kα source and the Bruker D8 Advance X-ray diffractometer, structural analyses of SnS thin films were carried out. Using a Horiba Labram HR Evo Raman spectrometer, Raman analysis was performed. The Intek UV- Vis spectrophotometer was used to optically characterize the annealed films. The 190 nm to 1190 nm wavelength range was used for the characterization. For UV radiation, deuterium was employed as the source, and tungsten for visible light. The films' morphology was examined using a FESEM (Field Emission Scanning Electron Microscope) (SUPRA 55 VP- 4132 CARL ZEISS). FESEM and energy dispersive spectroscopy (EDS) were both recorded to better understand the chemical composition.

3.1 Structural properties

The X-ray diffraction patterns of the SnS samples as prepared and those annealed at 100 °C, 150 °C, 200 °C, and 250 °C are displayed in figure 1. In SnS thin films, an intense peak was

observed at a 2θ value of 31.6 ° which, corresponds to the diffraction from the (0 1 3) plane for the films as prepared and those that were annealed at 100 °C. But for those annealed at 150 °C and 200 °C, the preferred orientation changes to the (1 1 0) plane related to the 2theta value of 30.5 °, while the other peaks determined at 26.9 °, 30.5 °, and 44.5 ° were indexed with the (0 1 2), (1 1 0) and (0 2 2) planes, respectively. All the peaks were indexed and compared with the standard ICDD data card of SnS (ICDD file no. 001-0984), and the crystal structure was found to be orthorhombic. The peaks become sharper and more intense on annealing, which shows a better crystallinity [24]. The samples annealed at 250 °C showed no peaks of SnS. This may be because the sulphur in the sample may have escaped at a temperature of 250 °C, causing the breaking of the stoichiometry of SnS.
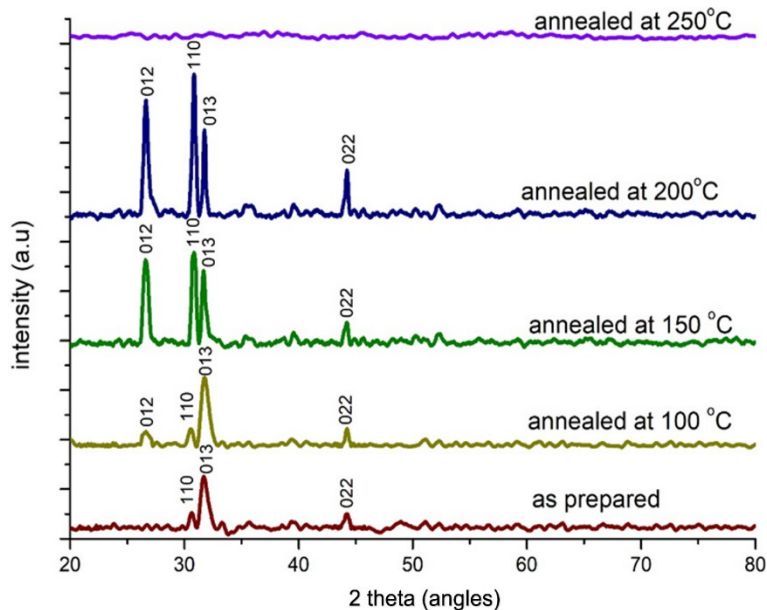
Fig. 1. X-ray diffraction pattern of SnS thin films.

3.1.1. Williamson–Hall method

The broadening of the XRD peaks arises from the crystallite size and lattice strain. The full width at half the maximum of the peaks (β) gives the measure of broadening.

$$\beta_{total} = \beta_{crystallite\ size} + \beta_{micro\ strain} \tag{1}$$

The FWHM due to crystallite size is given by the Scherrer equation, and that due to lattice strain by the microstrain equation. Substituting in equation (1), we get

$$\beta_{total} = \frac{k\lambda}{D\cos\theta} + 4\varepsilon\tan\theta \tag{2}$$

where k is the shape constant whose value is taken as 0.9, λ is the wavelength of the x ray used which is 1.5406 Å, D is the crystallite size and θ is the Bragg angle and ε is the microstrain of the lattice. This equation can be rearranged to produce a straight-line equation.

$$\beta_{total} = \frac{k\lambda}{D\cos\theta} + 4\varepsilon\frac{\sin\theta}{\cos\theta} \tag{3}$$

$$\beta_{total}\cos\theta = \varepsilon\,4\sin\theta + \frac{k\lambda}{D} \tag{4}$$

The equation (4) is a straight-line equation with the form y = mx + c, where m and c are the slope and intercept, respectively. A straight line will be produced by plotting a graph with 4sinθ on x-axis and β_{total}cosθ on y-axis with microstrain (ε) as slope and kλ/D as intercept[30,31]. The intercept can be used to calculate the crystallite size if the values of k and λ are known.

Figure 2 depicts the W-H plot of as-prepared and annealed samples at temperatures of 100 °C, 150 °C, and 200 °C. The crystallite sizes were found to be 37 nm, 38.8 nm, 47.7 nm, and 48.8 nm, respectively, for those as prepared and those with annealing temperatures of 100 °C, 150 °C, and 200 °C. The annealing helps to decrease the dislocations in the thin films and increases the crystallite size. The micro strain was determined to be 0.0043, 0.004, 0.0036, and 0.0035 for the as prepared and for annealing temperatures of 100 °C, 150 °C, and 200 °C, respectively. The reduction of the grain boundary, the elimination of deformation, and the removal of crystal defects could possibly be responsible for the increase in crystallite size, which indicates that the degree of perfection of the grains has increased. Thus, the reduction in the lattice imperfection reduces the strain in the lattice.
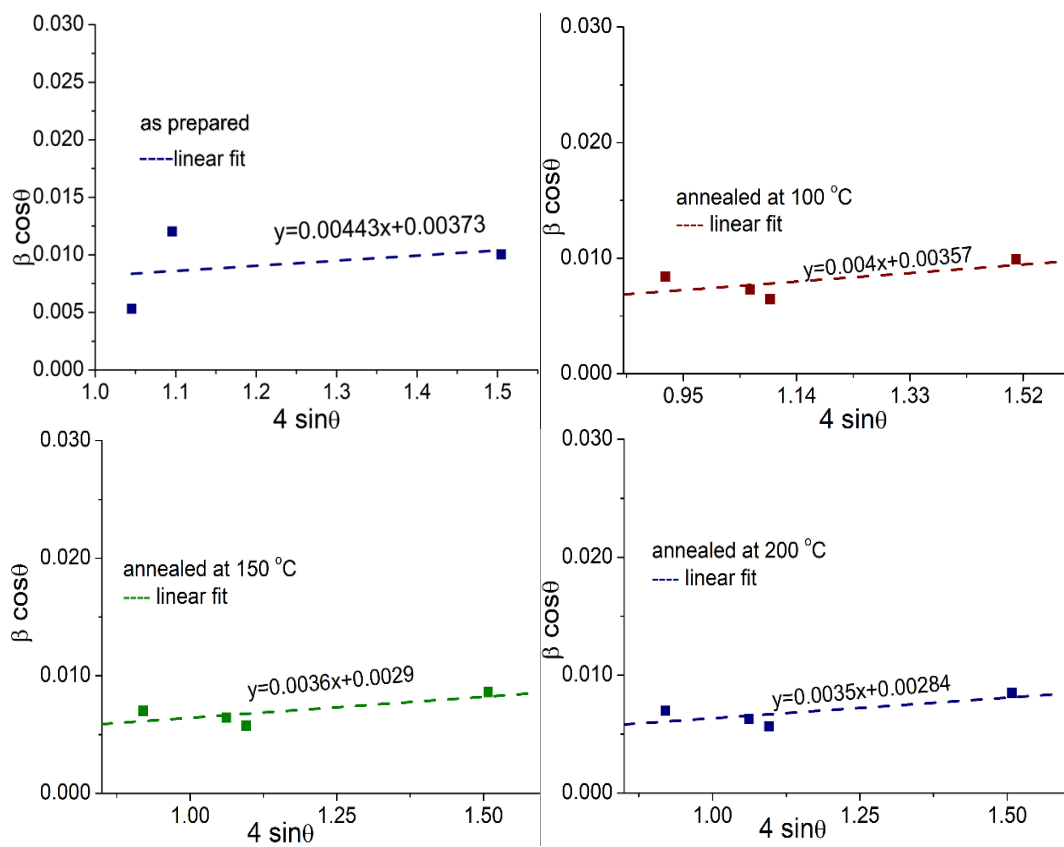
Fig. 2. Williamson-Hall plots of SnS thin films annealed at different temperature.

3.2. Raman analysis

Figure 3 displays the Raman spectra of SnS thin films. Prominent peaks related to SnS phonon modes are clearly observed at 94 cm^{-1} (A$_g$), 162 cm^{-1} (B$_{2g}$), and 220 cm^{-1} (A$_g$) in the spectra. The B$_{2g}$ mode represents the interaction through the interlayer b axis, whereas the A$_g$ mode indicates the symmetric Sn-S bond stretching in the a-c plane. Among the Ag modes identified, the peak at 220 cm-1 was attributed to the longitudinal optical (LO) mode, while the peak at 93 cm-1 was assigned to the transverse optical (TO) mode. [27][28]. The spectra are comparable to those of the bulk crystal and concur with past studies on SnS thin films. These results suggest that a SnS thin film with good crystallinity has been synthesized on the glass substrate The intensity of Raman lines was found to be high and sharp for the films annealed at 200 °C, which emphasizes improved crystallinity in these films and is consistent with the XRD

patterns in figure 1. It appears that the SnS peak shows the largest value when annealed at 200 °C. In contrast, the SnS peaks disappear at 250 °C or higher temperatures, while they have a considerable intensity at 200 °C and below.
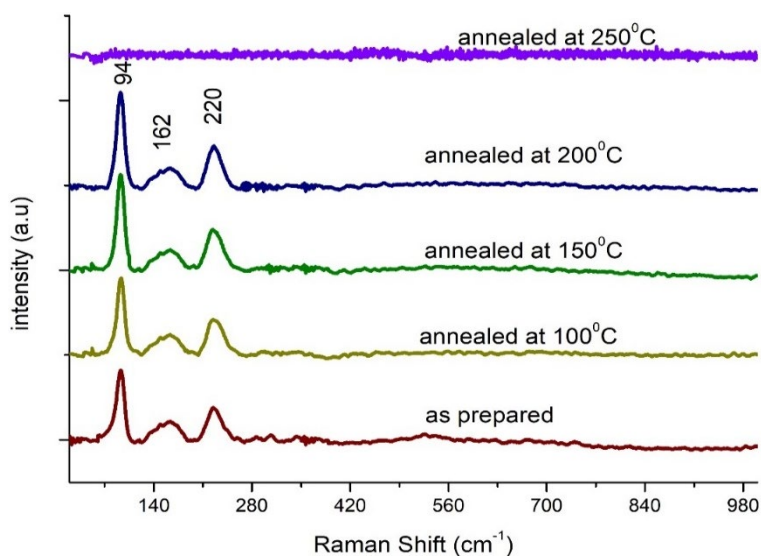
Fig. 3. Raman analysis of SnS thin films.

3.3. Optical properties

Figure 4 shows the absorption spectra (inset) and Tauc plot of SnS thin films for as prepared and annealed samples. The absorption spectra showed a red shift as the annealing temperature increased.
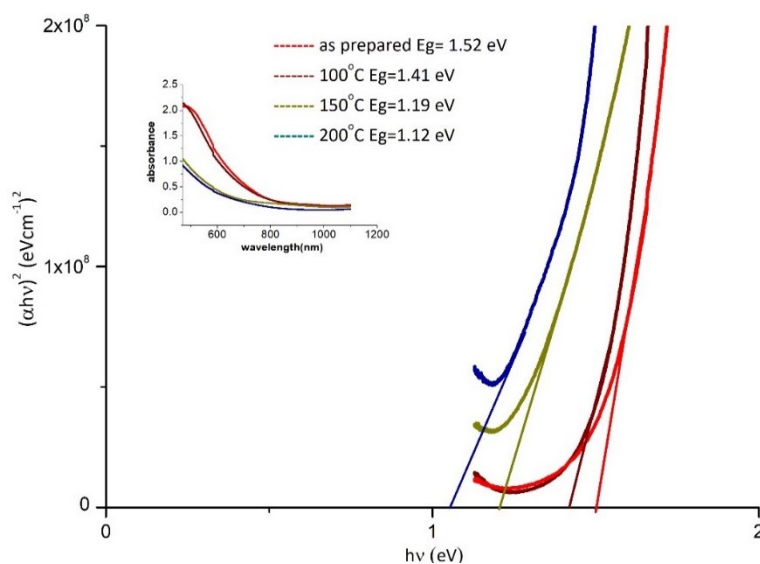
Fig. 4. Absorption spectra (inset) and Tauc plots of SnS films as prepared and annealed at different temperatures.

The tauc relation connecting bandgap energy and absorption coefficient (α) is given below.

$$\alpha h\upsilon = A (h\upsilon - Eg)^{n} \tag{5}$$

where, A is denotes a constant, hυ denotes photon energy, Eg denotes allowed energy gap, and n = ½ for allowed direct transition. For a direct bandgap semiconductor, tauc plot is drawn with hυ on x axis and $(\alpha h\upsilon)^2$ on the y axis. The presence of the linear portion in the curve indicates the presence of a direct optical transition in the material. The energy band gap can be determined by extrapolating the straight portion of the plot to the energy axis. The band gaps of SnS thin films were 1.52 eV, 1.41 eV, 1.19 eV and 1.12 eV corresponding to the as prepared and those annealed at 100 °C, 150 °C, and 200 °C, respectively. The energy gap increases with a decrease in the annealing temperature. The presence of grain boundaries in polycrystalline structures, which produce free carrier concentrations and the presence of potentials in the boundaries, may be the cause of the expanding energy gap. As a result, an electric field was created, which caused the band gap to widen. The film annealed at 200 °C has a band gap of 1.12 eV, which is appropriate for an absorber layer for effective light absorption.

3.4. Morphological studies

The FESEM images of the SnS films are shown in Figure 4. The morphology of SnS films (figure 5(a)-(d) revealed that as-deposited layers contain a lot of smaller needle-shaped grains, and as the annealing temperature rises, the grain size increases at the expense of the smaller crystals. The films exhibit considerable growth in three dimensions. These SEM photos clearly show that annealing causes grain development to switch from a needle-like to a plate-like structure. At 200 °C, the grains achieve their stable position with improved crystallinity. The reduction of grain boundaries is related to the improvement in crystallinity and grain size at higher temperatures. The films that have been annealed at 200 °C are uniform, smooth, and have a dense surface structure with larger grains than the films that were initially deposited.
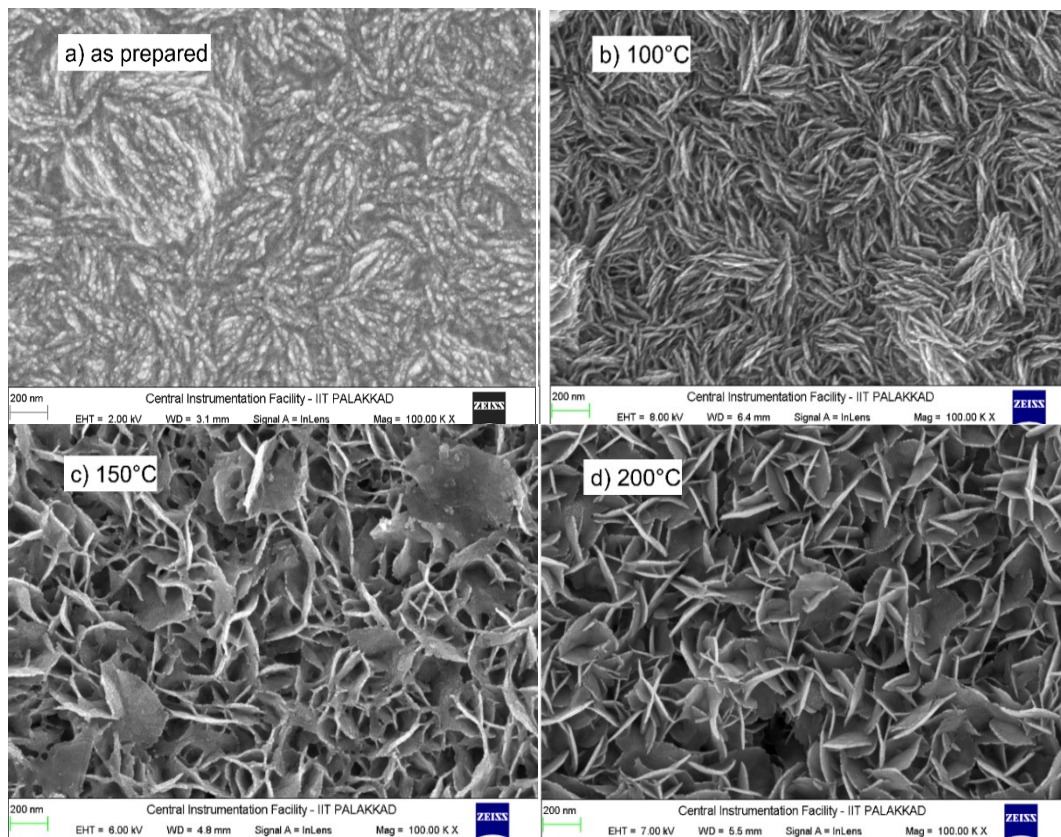
Fig. 5. Field emission scanning electron microscopy (FESEM) images of SnS.

3.5. Chemical studies

The EDS spectra of SnS thin films at various annealing temperatures are shown in Figure 6(a)–(d), demonstrating the presence of Sn and S peaks. The substrates employed give rise to the other unlabeled peaks. The spectra contained no further contamination peaks. The Sn/S atomic ratios found were higher than the predicted stoichiometric ratio of unity, indicating that the sample's surface was metal rich. As the annealing temperature increases, the atomic weight percentage of sulphur decreases. This is because the sulphur may have escaped from the sample with the increase in temperature.
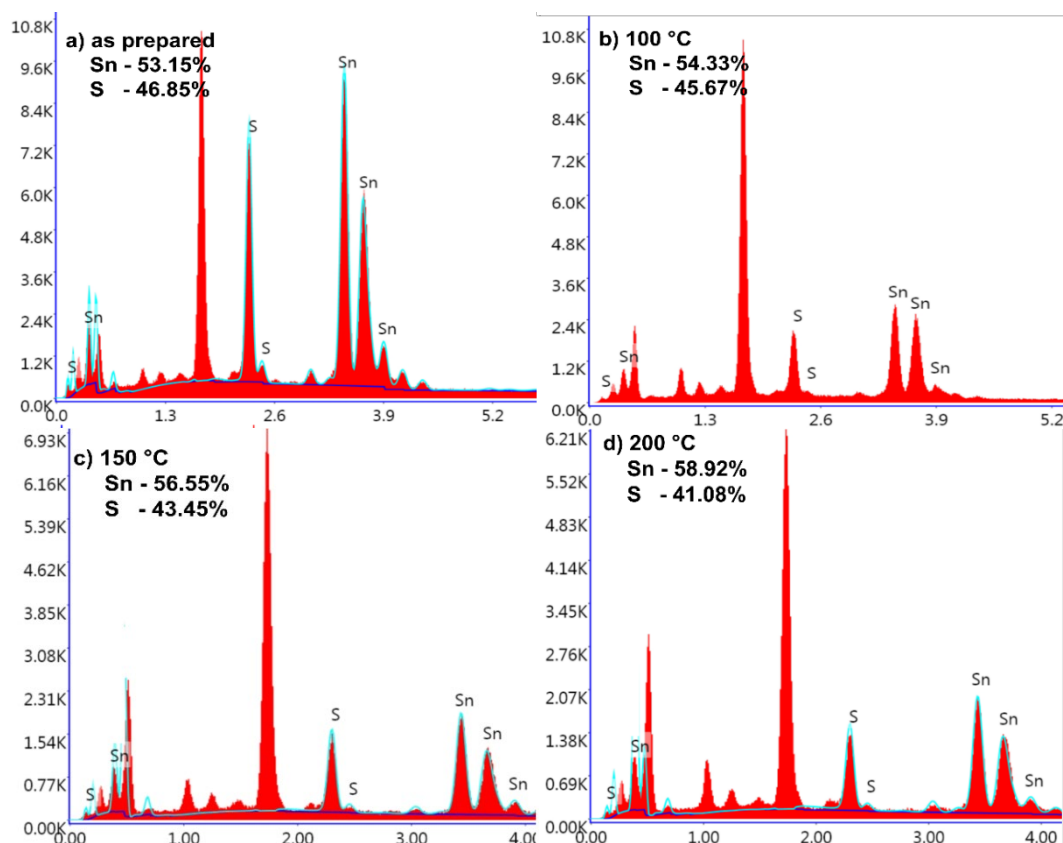
Fig. 6. EDAX images of SnS thin films annealed at different temperatures.

3.6. I-V Characterization

In the end, a SnS-based solar cell was created using ITO (Indium Tin Oxide) sold commercially as the back contact, CdS as the n-type semiconductor, SnS as the p-type semiconductor, and silver as the front contact (ITO/SnS/CdS/Ag). When the as-prepared SnS films were used as a p-type layer, their efficiency was 0.12×10^{-3} % and the photocurrent was in the order of 10^{-4} mA, which was very low. Then SnS film annealed at 200 °C was selected as the p-type material because it demonstrated the best crystallinity among the annealed films. Figure 7 displays the I-V Characterization for the aforementioned combination. The open circuit voltage (Voc), short circuit current (Isc), maximum power and current, fill factor, and efficiency are shown in the table that is displayed as an inset in the picture. A 0.015% efficiency was achieved. This is far better than the configuration made out of as-prepared SnS film. Still, the efficiency has to be improved.The insufficient CBO (Conduction Band Offset), carrier recombination, high resistivity of SnS thin film, sulphur vacancies, low thickness, etc. may all contribute to the poor performance[2], [29]. Another reason may be due to the loss of photons, which can be enhanced using anti-reflective coatings at the front and reflective coatings at the rear end of the configuration.
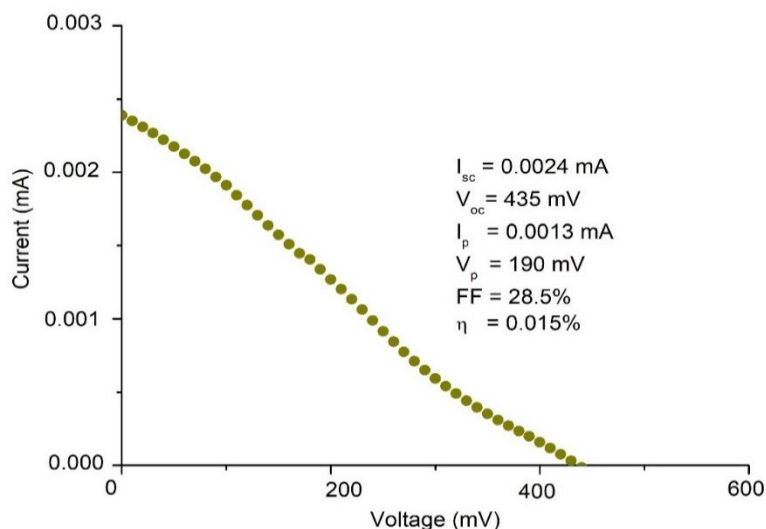
Fig. 7. I-V characteristics of SnS/CdS photovoltaic cell.

4. Conclusion

The chemically created SnS thin films were subjected to various annealing temperatures. The ideal annealing temperature for SnS was determined to be 200 °C. No peaks were visible in the films' annealed at 250 °C XRD or Raman spectra. The structural, morphological, optical, and chemical characterization demonstrated that variations in the annealing temperature led to modifications in the thin film properties. The films' crystallite size grew as the annealing temperature rose, according to structural analyses. It was discovered that when the annealing solution's temperature rose, the optical band gap shrank. With annealing, morphological tests revealed that the film became denser and the needle-shaped morphology changed to a plate-shaped one, increasing the grain size. The atomic weight of sulphur dropped as the annealing temperature rose, according to EDS spectra. ITO/SnS/CdS/Ag configuration were employed in the construction of photovoltaic cells, and a thin SnS film that had been annealed at 200 °C served as the absorber layer. The efficiency of the solar cell was found to be impacted by the annealing of the film. An increase in efficiency was seen by annealing the SnS thin film. This technique is an inexpensive way to produce SnS thin films for the absorber layer of solar cells.

References

[1] J. Y. Cho et al., Journal of Materials Chemistry A 8(39), 20658 (2020).
[2] J. A. Andrade-Arvizu, M. Courel-Piedrahita, O. Vigil-Galán, Journal of Materials Science: Materials in Electronics 26(7) , 4541 (2015); https://doi.org/10.1007/s10854-015-3050-z
[3] B. Singh, J. Singh, J. Kaur, R. K. Moudgil, S. K. Tripathi, Physica B: Condensed Matter 490, 49 (2016); https://doi.org/10.1016/j.physb.2016.03.006

[4] M. Ganchev, P. Vitanov, M. Sendova-Vassileva, G. Popkirov, H. Dikov, Journal of Physics: Conference Series 682(1) (2016); https://doi.org/10.1088/1742-6596/682/1/012019

[5] K. Hartman et al., Thin Solid Films 519(21) , 7421 (2011); https://doi.org/10.1016/j.tsf.2010.12.186

[6] B. S. Moon, J. H. Lee, H. Jung, Thin Solid Films 511-512 , 299 (2006); https://doi.org/10.1016/j.tsf.2005.11.080

[7] S. Mlowe et al., New Journal of Chemistry 38(12) , 6073 (2014); https://doi.org/10.1039/C4NJ01201A

[8] I. Y. Ahmet, M. S. Hill, A. L. Johnson, L. M. Peter, Chemistry of Materials 27(22) , 7680 (2015); https://doi.org/10.1021/acs.chemmater.5b03220

[9] B. Altiokka, A. K. Yildirim, Journal of the Korean Physical Society 72(6) , 687 (2018); https://doi.org/10.3938/jkps.72.687

[10] R. Mariappan, T. Mahalingam, V. Ponnuswamy, Optik 122(24) , 2216 (2011); https://doi.org/10.1016/j.ijleo.2011.01.015

[11] J. Johny, S. Sepulveda-Guzman, B. Krishnan, D. A. Avellaneda, J. A. Aguilar Martinez, S. Shaji, ChemPhysChem 18(9) , 1061 (2017); https://doi.org/10.1002/cphc.201601186

[12] J. C. Orlianges, C. Champeaux, P. Dutheil, A. Catherinot, T. M. Mejean, Thin Solid Films 519(21) , 7611 (2011); https://doi.org/10.1016/j.tsf.2010.12.139

[13] K. Santhosh Kumar, C. Manoharan, S. Dhanapandian, A. Gowri Manohari, Spectrochimica Acta - Part A: Molecular and Biomolecular Spectroscopy 115 , 840 (2013); https://doi.org/10.1016/j.saa.2013.06.112

[14] A. A. Aboud, A. Mukherjee, N. Revaprasadu, A. N. Mohamed, Journal of Materials Research and Technology 8(2) , 2021 (2019); https://doi.org/10.1016/j.jmrt.2018.10.017

[15] D. J. Desale et al., Adv. Appl. Sci. Res. 2(4) , 417 (2011).

[16] B. Ghosh, M. Das, P. Banerjee, S. Das, Applied Surface Science 254(20) , 6436 (2008); https://doi.org/10.1016/j.apsusc.2008.04.008

[17] H. Sattarian, T. Tohidi, S. Rahmatallahpur, Materials Science- Poland 34(3) , 540 (2016); https://doi.org/10.1515/msp-2016-0072

[18] U. Chalapathi, B. Poornaprakash, W. J. Choi, S. H. Park, Applied Physics A: Materials Science and Processing 126(8) , 1 (2020); https://doi.org/10.1007/s00339-020-03763-4

[19] S. John, V. Geetha, M. Francis, IOP Conference Series: Materials Science and Engineering 872(1) (2020); https://doi.org/10.1088/1757-899X/872/1/012139

[20] M. S. Su, C. Y. Kuo, M. C. Yuan, U. S. Jeng, C. J. Su, K. H. Wei, Advanced Materials 23(29) , 3315 (2011); https://doi.org/10.1002/adma.201101274

[21] T. Ben Nasr, N. Kamoun, M. Kanzari, R. Bennaceur, Thin Solid Films 500(1-2) , 4 (2006); https://doi.org/10.1016/j.tsf.2005.11.030

[22] V. S. Raut, C. D. Lokhande, V. V Killedar, International Journal of Engineering Research and Technology 10(1) , 568 (2017). [Online]. Available: http://www.irphouse.com

[23] S. John, V. Geetha, AIP Conference Proceedings 2162(October) (2019).

[24] N. Kabiri Samani, Z. Dehghani Tafti, H. A. Bioki, M. B. Zarandi, S. Shayegh, Optik 131 , 231 (2017); https://doi.org/10.1016/j.ijleo.2016.08.129

[25] A. S. Hassanien, A. A. Akl, Physica B: Condensed Matter 473 , 11 (2015); https://doi.org/10.1016/j.physb.2015.05.023

[26] E. R. Shaaban, N. Afify, A. El-Taher, Journal of Alloys and Compounds 482(1-2) , 400 (2009); https://doi.org/10.1016/j.jallcom.2009.04.033

[27] V. R. Minnam Reddy, S. Gedi, C. Park, M. R.w, R. R. Ramakrishna, Current Applied Physics 15(5) , 588 (2015); https://doi.org/10.1016/j.cap.2015.01.022

[28] E. Mellikov, V. Mikli, N. Revathi, O. Volobujeva, (October 2016) (2015).

[29] P. Sinsermsuksakul et al., Advanced Energy Materials 4(15) , 1 (2014); https://doi.org/10.1002/aenm.201400496